

Effects of polarization on laser-induced electron-ion recombinationT. Mohamed,^{1,*} G. Andler,² M. Fogle,¹ E. Justiniano,³ S. Madzunkov,¹ and R. Schuch^{1,†}¹*Department of Physics, Atomic Physics, Stockholm University, S-106 91 Stockholm, Sweden*²*Manne Siegbahn Laboratory, Stockholm University, S-10405 Stockholm, Sweden*³*Department of Physics, East Carolina University, Greenville, North Carolina 27858, USA*

(Received 16 September 2010; published 3 March 2011)

The polarization dependence of laser-induced radiative recombination (LIR) to D^+ ions was investigated in the electron cooler of the CRYRING storage ring. The LIR gain as a function of wavelength into $n = 3$ principal quantum states of deuterium was measured at laser beam polarization angles of 0° and 90° with respect to the direction of the motional electric field in the interaction region. For the case of the polarization vector parallel to the external field, there is a double-peak structure in the gain curve that indicates a polarization effect in the LIR process. The two polarization directions also reveal a different width for the respective gain curves, giving additional evidence for the polarization effect, clearly seen by the behavior of a defined polarization parameter. The obtained polarization effect indicates a high sensitivity in recombination processes to external fields.

DOI: [10.1103/PhysRevA.83.032702](https://doi.org/10.1103/PhysRevA.83.032702)

PACS number(s): 34.80.Lx, 42.25.Ja

I. INTRODUCTION

In the universe, most matter exists in the plasma stage, i.e., it consists of free ions and electrons. Recombination of electrons with ions is balanced by electron-impact ionization processes and the emission of electromagnetic radiation is controlled by inelastic electron-ion collisions. When a free electron is captured into a bound state in the ion, with the simultaneous emission of a photon, it is called radiative recombination (RR). This results in a continuum of photon energies determined by the electron energy distribution and the final quantum state. The basic theory of radiative transitions predicts that the recombination rate can be enhanced by stimulated photon emission using an external photon field such as that provided by an intense, monochromatic laser. Such a process is referred to as laser-induced recombination (LIR).

Considering the applied aspects and inherent fundamental processes in nature, it is important to study the dynamic behavior of recombination processes involving atomic constituents of matter. An in-depth knowledge of the physics governing these processes can also help us to prepare antimatter in the laboratory, e.g., for studying antihydrogen with high precision by recombining antiprotons with positrons [1]. In particular, LIR can be used to enhance weak recombination rates [2] by orders of magnitude compared to spontaneous RR [3] and also to prepare antihydrogen atoms in well-defined quantum states [4–6].

Heavy-ion storage rings equipped with electron coolers are powerful tools for measuring recombination processes at small relative energies. These electron coolers' primary function is to reduce the stored ion beam's emittance with a velocity-matched, cold-electron beam. The collinear electron beam also serves as an electron scattering target for near-zero energy electron-ion collisions for studies of recombination.

A disadvantage of electron coolers is that recombination photons are difficult to observe. This can, in part, be overcome by LIR, as a specific final state can be selected by setting the photon energy close to its binding energy. Stimulated photon emission is a resonant process, because it will only occur if the energy of the photons matches the energy difference $E_e - E_n$, where E_e and E_n are the energy of the electron and the energy of the bound state, respectively. The ratio between the induced recombination rate to the total spontaneous recombination rate over all final states n is referred to as the gain.

In the spontaneous recombination rate, close to zero relative electron collision energy, an enhancement over the theoretical predictions, has been observed in measurements at ion cooler storage rings. This has drawn attention both theoretically [7–11] and experimentally [12–16]. Such an enhancement effect was also investigated for the LIR process and was found by Schramm *et al.* [17] for C^{6+} . There, LIR shows a similar enhancement to that of spontaneous RR at low detuning energies of the merged ion and electron beams. LIR, therefore, represents an ideal tool to probe this effect with high resolution and additional parameters, such as polarization properties and energy detuning of a laser beam.

In fact, an additional effect that could be connected to the enhancement is the large contribution below threshold observed in LIR for specific laser tunings to defined principal quantum states [18–21]. Three possibilities could cause this below threshold gain: (1) the formation of quasibound Rydberg states when the ions pass through the toroid magnet of the electron cooler, which merges the electron beam with the ion beam. There is a transverse motional electric field in this area of the electron cooler that acts as a pulsed field (\sim ns). This field can induce electrons to be captured into high-lying states. The effect of such a field pulse has been used to explain the observed recombination enhancement [11,22]. Electrons in the high-lying states could be driven by the laser to a lower state and contribute thus to the below-threshold gain. A similar process has been observed in pulsed field recombination [23]. (2) The external electric fields in the interaction region of the electron cooler: The main sources of these external electric fields are (a) the field owing to the electron-beam space

*Permanent address: Physics Department, Faculty of Science, Beni-Suef University, Egypt.

†Author to whom correspondence should be addressed: schuch@physto.se

charge that depends on the displacement of the ion beam from the electron-beam axis and (b) the motional electric field $v \times B$, which arises from the small transverse component in the guiding magnetic solenoid field of the electron cooler. These fields distort the Coulomb potential of the ion such that a saddle-point is created. Electrons with energies between the saddle-point energy and the field-free threshold can recombine and contribute to the below-threshold gain. (3) Another possible recombination mechanism at low temperatures and/or high densities is collisional recombination [24], which is a general form of three-body recombination (TBR). In particular, TBR [9], including radiative deexcitation of electrons in Rydberg levels [15], or laser-induced deexcitation of Rydberg states can be effective to populate states below the threshold.

It can be expected that these different effects for causing the below-threshold gain will show different dependences on the polarization of the laser light and can thus be identified [scenarios (1) and (2) should show a polarization dependence on the orientation of the field, whereas in the case of (3) it should not be seen]. Therefore, in order to understand the contributions below threshold and the origin of the enhancement better, the effect from laser polarization on LIR into $n = 3$ states of deuterium was studied in this work. The gain was measured as a function of the relative photon energy to the photoionization threshold at 0° and 90° angles between the laser beam polarization and the direction of an external field.

II. EXPERIMENT

The experimental setup of the LIR measurement (Fig. 1) is described in detail in Ref. [19]. Briefly, the experiment was performed at the CRYRING storage ring at the Manne Siegbahn laboratory in Stockholm, Sweden. Deuterium (D^+) ions were produced in a plasmatron source, preaccelerated to 300 keV/amu with a radio-frequency quadrupole accelerator and injected into the ring where they were stored and accelerated to 7.82 MeV/amu. The ions were cooled by merging them with a cold, velocity-matched, electron beam of 20-mm radius in the electron cooler over a length 1 m. The electron cooler was set to provide an electron beam with a transverse temperature of $k_B T_\perp = 3$ meV and longitudinal temperature $k_B T_\parallel = 0.1$ meV. When the electron cooler was constructed around 1990, the longitudinal and transversal components of the magnetic field were measured [25]. Since then, the solenoid and toroid magnets were never taken apart, so the field components should have remained the same. The largest transverse component appears in the direction perpendicular to the plane of motion of the electrons in the transition region between the solenoid and toroid magnets (see Fig. 1). Using these measured values of transverse components and the ion velocity, we arrive at a motional electric field of 2 V/cm, perpendicular to the ion direction and in the plane of Fig. 1. We like to point out that we intentionally did not create an additional transverse field but worked under “normal conditions” in the cooler. That is where the rate enhancement occurs and we can see whether the below-threshold gain is connected to it.

Downstream from the cooler, a main dipole magnet separated the recombined ions from the circulating ion beam, and

they were detected with unity efficiency by a surface barrier detector (SBD) in the 0° beam line (see Fig. 1). At the given ion storage velocity, the magnetic field in the dipole magnet causes a field ionization of $n = 6$ and higher Rydberg states in the recombined deuterium atoms.

The laser system used in the experiment to drive the stimulated recombination process was a XeCl excimer pumped dye laser. The tuning range of the used dye, pyridine1 in dimethyl sulfoxide (DMSO), matches the recombination spectrum of D, $\Delta\lambda = 670\text{--}760$ nm. A narrow laser linewidth (~ 0.03 nm) was achieved with this system. The pulse duration of 17 ns, as given by the manufacturer, was confirmed by a photodiode measurement to an accuracy of 6%. The laser beam was transported to the center of the cooler (see Fig. 1) with an efficiency of $\sim 60\%$ using standard high reflective mirrors (M1–M4) and a focusing system (FS1) with antireflective-coated optics to control beam divergence. By using two highly reflecting mirrors (M3, M4) on precision motion and tilt actuators, the laser beam is elevated to match the height of the circulating ions and deflected into the vacuum chamber via an optical window. The position of the laser beam inside the interaction region was fully controlled by the M3 and M4 mirrors, whereas the laser beam size at the center of the electron cooler was controlled using a focusing system (FS2). A broadband polarization rotator (PR) with a clear aperture of 10 mm was used to rotate the laser polarization. Before the SBD located at 0° , a thin ($30\text{-}\mu\text{m}$) high reflecting quartz mirror (M5) was used to deflect the laser beam out of the vacuum in order to avoid dumping the laser beam into the light-sensitive SBD. The SBD housing was further shielded with by a thin reflective foil. The deflected laser beam was divided using a beam splitter. One part ($\sim 4\%$) was sent to a photodiode to obtain a timing signal. The residual part was used to record the laser power for beam alignment.

The measured output energy from the laser source was measured to $E_{LP}^{80\text{ Hz}} \approx 3\text{ mJ}$, with an accuracy of 10%, at a pump frequency of $f = 80$ Hz. This pump frequency of $f = 80$ Hz was found to be optimal for long-term efficiency for this laser system. After transport to the cooler, owing to optical losses, the energy of the laser pulse at the entrance to the vacuum system was $E_{\text{entr}}^{80\text{ Hz}} \approx E_{LP}^{80\text{ Hz}} \times 0.6 \approx 1.8$ mJ. In the overlap region, after losses in the entrance window, the energy was $E_{e\text{-cool}}^{80\text{ Hz}} \approx E_{\text{entr}}^{80\text{ Hz}} \times 0.95 \approx 1.7$ mJ. From the amount of energy per pulse in the interaction region and the laser pulse duration ($\tau_{LP} \approx 17$ ns), the power of the laser pulse can be estimated to be $P_{LP}^{80\text{ Hz}} \approx \frac{E_{e\text{-cool}}^{80\text{ Hz}}}{\tau_{LP}} \approx 0.1$ MW. In a first approximation, one may assume a constant laser beam area along the electron beam in the cooler with $S_{LP} = \pi R_{LP}^2 \approx 3.14 \times 10^{-2}$ cm² for a beam of radius $R_{LP} \approx 1$ mm. One then estimates a constant laser beam intensity along the interaction path of $I_{LP}^{80\text{ Hz}} \approx \frac{P_{LP}^{80\text{ Hz}}}{S_{LP}} \approx 3$ MW/cm².

The pump laser beam, however, has a Gaussian characteristic that is focused at the center of the e -cooler to a waist of approximately $\omega_m \approx 0.4$ mm, with a Rayleigh range close to $z_R \approx 1$ m, which matches the range of interaction of ions and electrons inside the electron cooler. This causes a varied laser-electron beam overlap and laser intensity along the interaction path. We found it necessary to take these details into account in determining the absolute gain.

The volume $V_{e-i} = \pi r^2 L$ of the cooled ion beam, filled with electrons, inside the e -cooler, has the form of a cylinder of length $L \approx 1$ m and cross section $S = \pi r^2$, where $2r \approx 1$ mm is its constant width. This volume is overlapped by the volume of the focused laser beam with a Gaussian distribution that can be evaluated from $V_{LB} = \int_{-L/2}^{L/2} \pi [f(z)]^2 dz$, where $f(z)$ is the beam waist function, expressed as $\omega(z) = \omega_0 \sqrt{1 + (\frac{z}{z_R})^2}$, where ω_0 stands for the beam waist at focus and z_R for the Rayleigh range. At the entrance of the interaction region, $z = -\frac{L}{2}$, $f(-\frac{L}{2}) \approx r$, the dimension of the cooled ion beam. So that the volume of the focused laser beam is $V_{LB} = \pi \int_{-L/2}^{L/2} \omega_0^2 [1 + (\frac{z}{z_R})^2] dz$, and thus the ratio between laser and ion-beam volumes in the interaction range is $\eta = \frac{V_{LB}}{V_{e-i}} = 0.2$. The ratio between cross sections of laser and ion beams varied along the electron cooler and reaches one at the entrance and the exit of the electron cooler, where the areas of the laser and ion beams are equal. Because the laser intensity also varies along the electron cooler for a given laser power, it is necessary to convolute the laser intensity along the electron cooler with the overlap. This overlapping laser intensity is used to calculate the gain, which is discussed later. We adjusted and measured the focus profile by first transporting the laser beam next to the cooler. From this measurement and the beam scraper measurements (see below), the parameters and error in the overlapping laser intensity was estimated to be 10%.

From the D^+ velocity one determines the laboratory wavelength corresponding to the (field-free) binding energy of the deuterium $n = 3$ state to be 721.05 nm (vacuum value). The laser wavelength was scanned over a range of 720.7–722.7 nm,

whereby the Doppler shift transforms these wavelengths into a center-of-mass range of 819.61–820.75 nm, which includes the $n = 3$ threshold wavelength of 820.36 nm. For each wavelength step in the scan, $\sim 5 \times 10^4$ pulses were fired by the laser. A coincidence requirement between the SBD pulses and the laser pulses was set using a time-to-amplitude converter (TAC). The laser pulse detected by a photodiode was used as a start signal and the stop signal was triggered by the arrival of a deuterium atom at the SBD.

The most challenging aspect of the LIR experiment is obtaining an overlap of the laser beam (~ 0.5 – 1 mm radius) with the ion beam (~ 0.5 mm radius). This alignment was done using two sets of horizontal and vertical scrapers situated in the 0° beam line following the dipole magnet downstream from the cooler. These scrapers were situated such that the first was ~ 2 m from the center of the interaction region with a separation of 1 m between the scraper positions. The relative horizontal and vertical positions of the ion beam (actually a projection of the ion beam formed by recombined atoms) were measured using a rate meter, showing the rate of neutral particles detected by the SBD at the end of the 0° beam line. Each scraper was moved until the rate dropped to half of its initial value and the setting of the manipulator was recorded for both x and y positions. For the laser beam positions, a power meter was used to monitor the laser power in the same way as in the case of the rate of neutral particles. These relative beam position measurements could be taken simultaneously for each beam individually. The position and angle of the laser beam was changed until the overlap with the ion beam was achieved. This overlap was clearly detected by the maximum

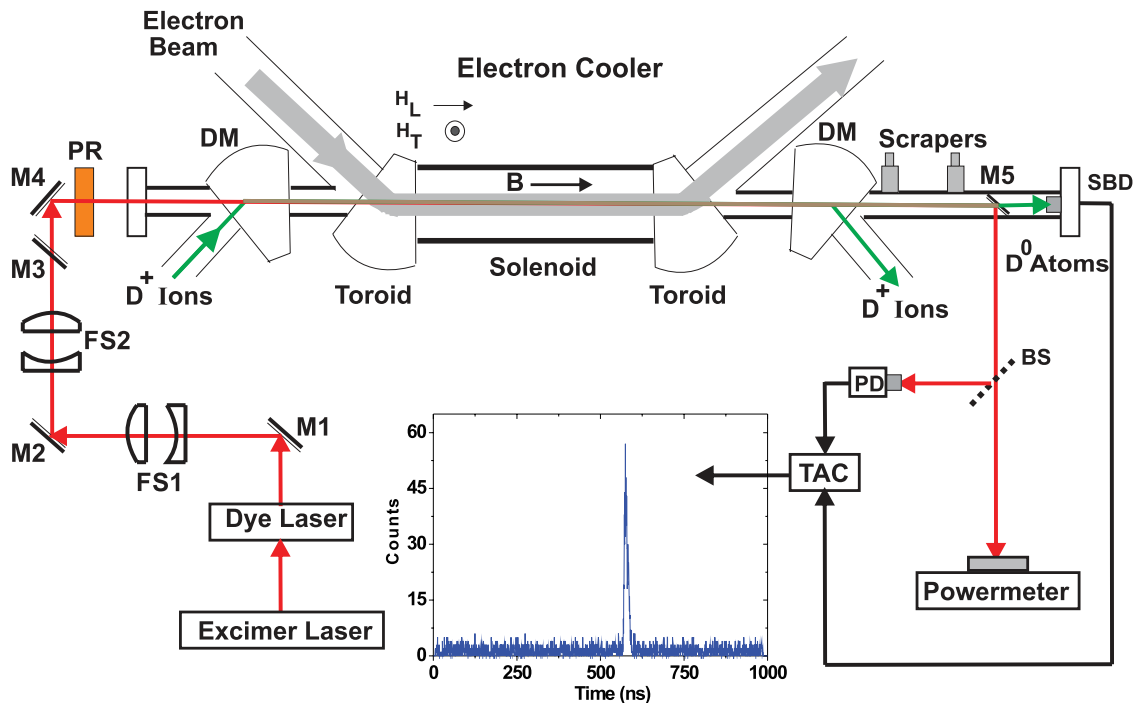


FIG. 1. (Color online) Schematic diagram of experimental setup for LIR measurements. M1, M2, M3, and M4 are highly reflecting mirrors, M5 is a thin quartz mirror, FS1 and FS2 are the focusing systems, BS is the beam splitter, PR is the polarization rotator, DM are the ring dipole magnets, H_L and H_T are the longitudinal and transversal components of the magnetic field in the transition region between the solenoid and toroid magnets, TAC is the time-to-amplitude converter, and SBD is the surface barrier detector. The inset shows a time-of-flight spectrum from the TAC (see text).

coincidence rate of laser pulses with neutral particles in the SBD.

III. RESULTS

In the 1- μ s time window of the TAC, the time peak signature of the induced recombination was seen as a sharp peak clearly above the background level given by the atoms formed through spontaneous recombination (see Fig. 1). The width of the time peak (≈ 40 ns) is determined by the duration of the laser pulse (≈ 17 ns) and the variation in the time of flight of the ions within the length of the interaction region (≈ 23 ns) to the SBD. At a laser pulse repetition rate of 80 Hz, an ion current of 100 μ A, and an electron current density of 1.1×10^7 cm $^{-3}$, the typical coincident signal count rate was ≈ 0.1 counts/s.

For each wavelength in the scan range, we extract the corresponding coincident time peak by gating the total coincidence time peak, on the individual wavelengths in the scan range. The gain factor for each wavelength can be obtained [18] only from experimental parameters:

$$G = \frac{N - N_{\text{spont}} \Delta t}{N_{\text{spont}} T}. \quad (1)$$

In this expression, N is the number of total counts under the time peak, N_{spont} is the average number of spontaneous recombination counts per channel in an interval around the time peak, Δt is the width of the time peak for which N is calculated, and T is the laser pulse duration. Thus, the numerator of Eq. (1) represents the number of induced counts under the time peak while the denominator represents the number of spontaneous counts in a time interval equal the laser pulse duration.

A measured gain curve as a function of the relative photon energy is displayed in Fig. 2. The laser polarization was set to 90° (perpendicular polarization) with respect to the direction of the motional electric field. The gain factor starts to rise at -1.4 meV below the expected field free threshold. It reaches a maximum of 67 ± 10 at -0.5 meV, below the threshold, and

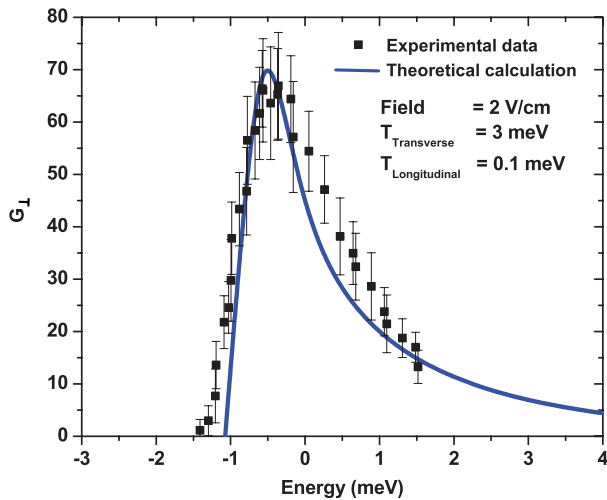


FIG. 2. (Color online) Gain spectrum for LIR into $n = 3$ of deuterium for laser beam polarization perpendicular to the motional electric field, $v \times B$. The solid curve shows the theoretical prediction in absolute scale.

falls off to its half value within ~ 0.6 meV, and then decreases slowly with increasing relative photon energy. The error in the energy scale of the measured gain curve is estimated to be ± 0.15 meV, owing to the uncertainty in the storage ring length that is used in conjunction with the circulating frequency to determine the velocity of the ions. The statistical error in the measured gain values is a combination of the error in determining the number of induced counts and the variation of the spontaneous recombination background.

As in earlier experiments, gain of the induced recombination process (Fig. 2) is observed also at photon energies below the photoionization threshold for the estimated external electric-field strength. This could indicate that electrons become bound in high Rydberg levels during the interaction of deuterium ions with the electrons and are stabilized against field ionization by stimulated radiative transition into $n = 3$. Without this radiative stabilization, deuterium atoms in high Rydberg levels would be field ionized by the dipole magnet following the cooler before reaching the SBD. It is expected that this fraction of stimulated stabilization is independent of the laser polarization owing to the large number of states involved.

Theoretically, the LIR gain factor has been given by Refs. [18] and [20]. The effect from the motional electric field on the gain is calculated by averaging the gain at each wavelength over the angle between the electron trajectory and the motional electric-field direction [18]. To describe the effect from the laser polarization, the LIR gain was modeled as given in Ref. [21], where the gain curve is derived from the differential photoionization cross section $\sigma_{\text{nl}}^{\text{ph}}$ using the detailed balance principle as given in Ref. [26]. In this model the differential photoionization cross section is averaged over the angle between the laser polarization vector and the electric-field direction. Then the effect from the motional electric field and the different laser polarization on LIR gain can be given as

$$G_n(\varepsilon) = \frac{R_n^{\text{ind}}}{R_{\text{spont}}} = \sum_{\ell=0}^{n-1} G_{\text{nl}}^0 \int_{\varphi=0}^{\pi} \int_{\theta=0}^{2\pi} \sigma_{\text{nl}}^{\text{ph}}(\chi) \sin(\varphi) \times \int_{E_\gamma=E_0-E_{\text{sp}} \sin \frac{\varphi}{2}}^{\infty} f(\varepsilon_t, \varphi, \vartheta) g(E_\gamma) dE_\gamma d\varphi d\vartheta, \quad (2)$$

where the factor G_{nl}^0 contains contributions from spontaneous recombination, R_{spont} , the laser intensity, and laser frequency. $f(\varepsilon_t, \varphi, \vartheta)$ describes the flattened velocity distribution of the electrons, φ is the angle between the electron momentum vector and the laser polarization vector, and ϑ is the angle between the electron momentum vector and the direction of propagation of the ion. $g(E_\gamma)$ is a normalized Gaussian that accounts for the linewidth of the laser. We apply this approximation in the threshold region, just above the saddle-point energy, where the electron momentum vector is in the direction of the external field. The angle χ is thus between the laser beam polarization and the direction of the motional electric field $v \times B$, and $\varepsilon_t = E_\gamma - E_0 - E_{\text{sp}} \sin \frac{\varphi}{2}$, where the E_{sp} term accounts for the fact that an external electric field lowers the ionization threshold [18].

The solid curve in Fig. 2 represents the calculated gain in absolute scale given by Eq. (2) for laser beam polarization perpendicular to the motional electric field. In this calculation

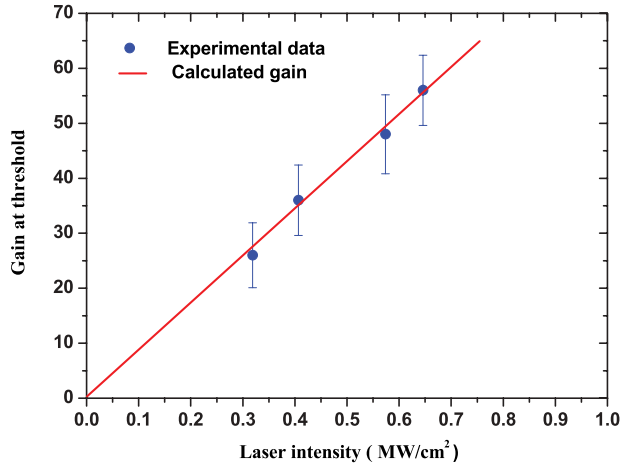


FIG. 3. (Color online) The measured gain as a function of the laser pulse intensity at $\lambda = 721.5$ nm. The solid line shows the calculated gain in absolute scale as a function of intensity.

the experimental parameters such as the electron-beam temperatures of $T_{\perp} = 3$ meV and $T_{\parallel} = 0.1$ meV, the overlapping laser intensity of 0.6 MW/cm², and a transverse component of the motional electric field of 2 V/cm were used. The longitudinal component is not taken into account in the calculated gain because it is much smaller than the transversal. The solid curve reaches zero at the saddle-point energy $E_{sp} = -1.07$ meV. The absolute good agreement between the calculated gain and the measured gain was obtained when the laser beam along the electron cooler was considered as a Gaussian beam of variable width, as been discussed earlier. The total systematic error is according to the contributions mentioned above in the order of 15%.

Figure 3 shows the measured gain as a function of the laser intensity that is varied from 0.3 to 0.6 MW/cm² and at maximum gain, i.e., a photon wavelength of $\lambda = 721.5$ nm. The calculated gain (solid line) is obtained by using the relation given in Ref. [2] and agrees well in absolute scale with the measured gain. The laser intensity is below the saturation intensity (≈ 2 MW/cm²) for these measurements, resulting in a gain well below a saturation gain of ≈ 300 ; thus it shows a linear dependence.

The gain curve, obtained using a laser polarization parallel to the direction of the motional electric field, is shown in Fig. 4. The gain factor starts to rise at -1.5 meV, below the expected field-free threshold. It reaches a maximum of 70 ± 7 at -0.3 meV, falls off to half maximum within ≈ 0.8 meV, and then decreases with increasing relative photon energy. The solid curve, representing the theoretical calculation in absolute scale, reaches zero at the saddle-point energy, $E_{sp} = -1.07$ meV.

The experimental data for the 0° polarization shows an indication of a double-peak structure with a dip at ~ -0.6 meV relative photon energy. Such a dip does not exist on the gain curve of the perpendicular polarization in Fig. 2. The two polarization directions have quite different parameters for the respective gain curves, e.g., widths of 1.11 ± 0.17 and 0.79 ± 0.05 meV for parallel and perpendicular polarizations, respectively. In order to investigate the significance of the

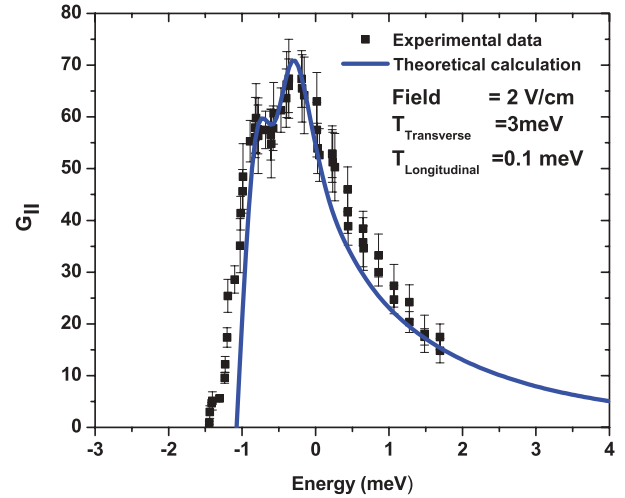


FIG. 4. (Color online) Gain spectrum for LIR into $n = 3$ of deuterium for laser beam polarization parallel to the motional electric field, $v \times B$. The solid curve shows the theoretical prediction of the gain in absolute scale.

observed polarization difference, we consider a polarization parameter, defined as

$$p = \frac{G_{\perp} - G_{\parallel}}{G_{\perp} + G_{\parallel}}. \quad (3)$$

This defined parameter varies between $p = 0$ (no polarization effect or $G_{\perp} = G_{\parallel}$) and $p = 1$ or -1 (maximum polarization, $G_{\parallel} = 0$ or $G_{\perp} = 0$, respectively). From the absolute theoretical gains displayed in Figs. 2 and 4, the theoretically estimated polarization parameter p is obtained by applying Eq. (3) and is represented by the solid curve in Fig. 5. The experimental gains were obtained from several runs where the scan steps were different and the steps also changed in the range of λ from 0.05 to 0.2 nm. Therefore, for obtaining the polarization parameters from the experimental gain values, we had to average one of them (the gain for laser polarization perpendicular to the electric field) in certain intervals as they were not always measured at exactly the same wavelength.

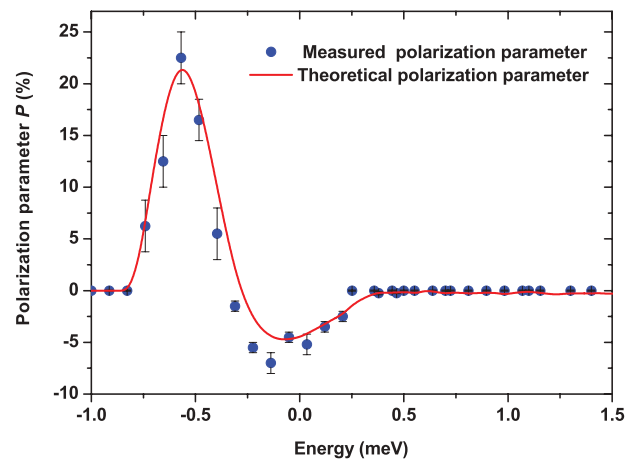


FIG. 5. (Color online) Polarization parameter P for LIR into $n = 3$ of deuterium as a function of the relative photon energy. The solid curve shows the theoretical prediction of P .

As seen in Fig. 5, the measured polarization parameter is well described by the calculated curve, and shows a clear evidence for the polarization effect in LIR. The measured polarization parameter shows also that G_{\perp} and G_{\parallel} are different by a maximum value of 20%, which appears at the dip of measured parallel polarization. From this overall good agreement, one can conclude that the observed effect is owing to this external electric field in the interaction region.

IV. CONCLUSION

We measured the polarization dependence of laser-induced recombination into $n = 3$ of D using a laser with a narrow

linewidth. The polarization was changed with respect to a small motional electric field of ~ 2 V/cm, transverse to the ion motion. For the polarization parallel to the external field there is a double-peak structure in the gain curve with a dip at ~ -0.6 meV relative photon energy with respect to the threshold for stimulated emission to $n = 3$. Clear evidence for the influence of the laser polarization on LIR is obtained from a polarization parameter. From the overall good agreement between the measured and calculated polarization parameters, we conclude that the observed induced recombination below threshold is owing to the small transverse electric field in the interaction region that populates high-lying Rydberg states and not from collisional or three-body recombination.

-
- [1] M. Amoretti *et al.*, *Nature (London)* **419**, 456 (2002); G. B. Andresen *et al.*, *ibid.* **468**, 673 (2010).
- [2] R. Neumann, H. Poth, A. Winnacker, A. Wolf, *Z. Phys. A* **313**, 253 (1983).
- [3] Alfred Müller and Andreas Wolf, *Hyperfine Interact.* **109**, 233 (1997).
- [4] G. Gabrielse *et al.*, *Phys. Rev. Lett.* **89**, 213401 (2002).
- [5] G. Gabrielse *et al.*, *Phys. Rev. Lett.* **89**, 233401 (2002).
- [6] J. Walz, P. Fendel, M. Herrmann, M. König, A. Pahl, H. Pittner, B. Schatz and T. W. Hänsch, *J. Phys. B* **36**, 649 (2003).
- [7] Y. Hahn and P. Krstic, *J. Phys. B* **27**, L509 (1994).
- [8] Y. Hahn and J. Li, *Z. Phys. D* **36**, 85 (1996).
- [9] M. Pajek and R. Schuch, *Hyperfine Interact.* **108**, 185 (1997).
- [10] G. Zwicknagel, C. Toepffer and P.-G. Reinhard, *Hyperfine Interact.* **99**, 285 (1996).
- [11] C. Heerlein, G. Zwicknagel, and C. Toepffer, *Phys. Rev. Lett.* **89**, 083202 (2002).
- [12] H. Gao, D. R. DeWitt, R. Schuch, W. Zong, S. Asp, M. Pajek *et al.*, *Phys. Rev. Lett.* **75**, 4381 (1995).
- [13] H. Gao, S. Asp, C. Biedermann, D. R. DeWitt, R. Schuch, W. Zong, and H. Danared, *Hyperfine Interact.* **99**, 301 (1996).
- [14] U. Schramm, T. Schüssler, D. Habs, D. Schwalm, and A. Wolf, *Hyperfine Interact.* **99**, 309 (1996).
- [15] H. Gao, R. Schuch, W. Zong, E. Justiniano, D. R. DeWitt, H. Lebius, and W. Spies, *J. Phys. B* **30**, L499 (1997).
- [16] G. Gwinner *et al.*, *Phys. Rev. Lett.* **84**, 4822 (2000).
- [17] U. Schramm, A. Wolf, T. Schüssler, D. Habs, D. Schwalm, O. Uwira, J. Linkemann, and A. Müller, *Hyperfine Interact.* **108**, 273 (1997).
- [18] U. Schramm, J. Berger, M. Grieser, D. Habs, E. Jaeschke, G. Kilgus, D. Schwalm, A. Wolf, R. Neumann, and R. Schuch, *Phys. Rev. Lett.* **67**, 22 (1991).
- [19] S. Asp, R. Schuch, D. R. DeWitt, C. Biedermann, H. Gao, W. Zong, G. Andler, and E. Justiniano, *Nucl. Instrum. Methods B* **117**, 31 (1996).
- [20] A. Wolf, in *Recombination of Atomic Ions*, NATO ASI, Series B: Physics, edited by W. G. Graham, W. Fritsch, Y. Han, and J. A. Tanis (Plenum, New York, 1992), Vol. 296.
- [21] W. Spies, P. Glans, W. Zong, H. Gao, G. Andler, E. Justiniano, M. Saito, and R. Schuch, *Hyperfine Interact.* **114**, 237 (1998).
- [22] M. Hörndl, S. Yoshida, K. Tökési, and J. Burgdörfer, *Phys. Rev. Lett.* **93**, 209301 (2004).
- [23] C. Wesdorp, F. Robicheaux, and L. D. Noordam, *Phys. Rev. A*, **64**, 033414 (2001).
- [24] D. R. Bates, A. E. Kingston, and R. W. P. McWhirter, *Proc. R. Soc. London, Ser. A* **267**, 297 (1962); **270**, 155 (1962).
- [25] H. Danared, *Phys. Scr.* **48**, 405 (1993).
- [26] M. Pajek and R. Schuch, *Phys. Rev. A* **45**, 7894 (1992).